

# TECHNICAL SCIENCES

## SEARCHING OF AERODYNAMIC STRUCTURE AROUND BUILDINGS HAVING DISTINCT GEOMETRIC DESIGN PARAMETERS

**Gölbaşı D.**

*Assist. Prof. Dr., Department of Mechanical Engineering, Faculty of Engineering,  
Sivas Cumhuriyet University, Sivas, Türkiye*

**Buyruk E.**

*Prof. Dr., Department of Mechanical Engineering, Faculty of Engineering,  
Sivas Cumhuriyet University, Sivas, Türkiye*

**Karabulut K.**

*Assoc. Prof. Dr., Department of Electric and Energy, Sivas Vocational School of Technical Sciences, Sivas  
Cumhuriyet University, Sivas, Türkiye*

**Ağbaba Ya.**

*Msc., Department of Mechanical Engineering, Institute of Science, Sivas Cumhuriyet University, Sivas, Türkiye*

<https://doi.org/10.5281/zenodo.17609042>

### Abstract

Building aerodynamics is a vital interdisciplinary field that investigates the interactions between wind flow and building surfaces. In this study, flow structures around three building models with a 30° slope-10 cm × 5 cm × 5 cm, 5 cm × 5 cm × 10 cm, and 5 cm × 5 cm × 5 cm-were experimentally analyzed using Particle Image Velocimetry (PIV). Instantaneous velocity fields were measured, and time-averaged velocity distributions  $\langle V \rangle$  and streamlines ( $\psi$ ) were computed. The results show that wind separation at edges and corners generates recirculation zones along façades, side walls, rear, and roof regions, with elevated turbulence in the shear layers. Boundary layer thickness decreases toward the side edges, shortening downstream separation regions, while high turbulent kinetic energy is concentrated in wake vortices. Rotation of elongated building models significantly enlarged the wake vortices and influenced surrounding flow, whereas rotation of the cubic model had negligible effect. These findings highlight that building orientation strongly affects wake formation, particularly for elongated geometries.

**Keywords:** Building aerodynamics, Particle Image Velocimetry (PIV), Wake vortices, Flow separation

### Introduction

Building aerodynamics is an important interdisciplinary research field that examines the effects of wind flow on building surfaces and their immediate surroundings. Increasing population density, intensive construction, and the proliferation of tall buildings with complex geometries underscore the critical role of wind loads in building performance (Blocken, 2014). Reyes and colleagues (2015) applied the Particle Image Velocimetry (PIV) method in a building–wind tower configuration to study airflow. To measure flow distribution by simulating natural ventilation, they conducted wind tunnel experiments with scaled models. Subsequently, the obtained PIV data were compared with RANS-based CFD simulations, and good agreement was observed in the comparison results. As a result, the study demonstrated that PIV is a reliable experimental validation tool for improving the design of wind towers. Furthermore, it recommended the use of the PIV technique in natural ventilation analysis. Sugahara et al. (2017) investigated the effects of installing air-cooled packaged air conditioners used in small and medium-sized buildings on the roof and on airflow in their study. The study used Particle Image Velocimetry (PIV) experiments conducted with scaled models to evaluate the effect of the position between the devices on airflow characteristics. Furthermore, the experimental data obtained were compared with Computational Fluid Dynamics (CFD) simulations, demonstrating that CFD can represent airflow close to the actual situation. The

results reveal that the optimal configuration of rooftop units is crucial for improving energy efficiency. Liu and et al. (2021) investigated the effects of horizontal and vertical ribs on local and global wind loads on the façades of tall buildings. The study analyzed models with six different rib configurations using experimental pressure measurements and high-frequency Particle Image Velocimetry (PIV). The results showed that horizontal ribs reduced the height of the leading stagnation point, while vertical ribs reduced turbulence intensity in the shear layer and near-wake region, thereby decreasing the fluctuating wind pressure on the side and leeward surfaces. Furthermore, the effect of the protrusions on the average wind force was evaluated by controlling the wake vortex length (L) and local wake width (W), and it was found that the optimal configuration is effective in reducing side wind forces. Liu et al. (2024) investigated natural convective flows caused by high heat loads in industrial buildings using a large-scale test rig and 2D PIV. The results showed that the air flow near the walls was anisotropic, the flow at the center was isotropic, and turbulence and fluctuations varied depending on the Rayleigh number. The study provides fundamental data for optimizing air distribution design in industrial buildings. Bagheri and et al. (2023) investigated the effects of natural ventilation on indoor air exchange rate and flow velocity in single-sided and cross ventilation modes. Experiments conducted using a water bath model and Particle Image Velocimetry (PIV) found that flow velocity was 18-32%

higher at low inlet levels in single-sided ventilation mode, but cross ventilation mode provided 28% higher flow when windows were positioned high. The tests showed that cross ventilation creates a higher air exchange rate than single-sided ventilation due to the lift force effect and that the air exchange rate increased by 71.75% when high-level outlet openings were used. Setio and et al. (2020) investigated wind loads on structures built between high-rise buildings in urban areas in Indonesia. Wind tunnel experiments using a simplified four-symmetric high-rise building model and Particle Image Velocimetry (PIV) were conducted to evaluate the effects of different attack angles and inter-building distances. The results showed that the interaction flow between buildings increased wind speed, that building distance altered cross-flow behavior, but that the attack angle did not affect the amplification factor. It was found that wind speed increased by 7-44% due to street canyons and that the highest amplification occurred at a  $0^\circ$  attack angle. Tominaga and colleagues (2015) investigated the airflow around isolated triangular-roofed buildings with different roof slopes. Wind tunnel experiments measured time-averaged velocity, turbulent kinetic energy, and pressure coefficient, followed by validation using RANS-based CFD simulations. The results showed that the simulations agreed well with the measured values for flow-direction velocities (15% deviation), but that transient vortex effects in the rear regions of the building could not be fully captured with steady RANS. Furthermore, it was found that the roof slope had a significant effect on the flow field around the building, and that the difference between slopes of 3:10 and 5:10 was greater than the difference between 5:10 and 7.5:10. Albuquerque and colleagues (2020) experimentally and numerically investigated pumped natural ventilation in an isolated building. Wind tunnel experiments and PIV measurements showed that pumped ventilation is a periodic and three-dimensional oscillatory phenomenon. In numerical simulations, LES accurately predicted ventilation rates, while URANS produced significantly lower values. The efficiency obtained with LES was found to be in the range of 0.60-0.75. Kim et al. (2019) experimentally investigated the **wind flow around two connected buildings**. Models with different gap distances were analyzed using **Particle Image Velocimetry (PIV)** and **Proper Orthogonal Decomposition (POD)**. Results showed that for side-by-side arrangement with a small gap, a single vortex street and biased flow formed, while a larger gap led to two independent vortex streets. In tandem arrangement ( $\alpha = 90^\circ$ ), the shear layer street influenced the entire system, whereas for  $\alpha = 0^\circ$ , the gap distance significantly affected the flow patterns. When the gap was two-thirds of the building width, the maximum mean wind velocity around the buildings was observed.

Liu et al. (2023) investigated the effects of **horizontal ribs** on wind impact reduction for tall buildings using a **Large Eddy Simulation (LES)** approach under atmospheric boundary layer flow. Results showed that horizontal ribs significantly **suppress the formation of separation vortices** near the side walls and increase vortex size in the wake. The ribs obstruct vertical flow near the façade, creating small recirculation zones and localized flow concentration between adjacent ribs, which leads to notable changes in the near-wall flow pattern. These modifications in near-wall flow result in significant variations in **wind pressure distribution and wind forces**. Continuous ribs can induce a “zig-zag” pattern in the mean pressure along the building height and reduce fluctuating lift forces by up to 27%, whereas discrete ribs have relatively weak effects on wind forces. Han et al. (2022) investigated **thermal plumes from high-rise façades** under windless conditions using a scaled model and **PIV**. Results showed that vertical wind speed increases with height while temperature remains nearly constant, and horizontal air speed peaks near  $y/D = 0.1$ , with thermal effects confined to roughly half the building thickness.

#### Material and Method

In this study, experiments were conducted using Particle Image Velocimetry (PIV) within both closed-loop and open-surface water channels. The experimental setup was constructed from fiberglass and comprised two water reservoirs connected by a transparent acrylic test section. The test section measures 750 mm in height, 1000 mm in width, and 9000 mm in length. Water circulation between the reservoirs is maintained by a 15 kW centrifugal pump, whose rotational speed is controlled via a frequency-regulated drive, enabling experiments at varying flow rates. The pump draws water from the downstream reservoir and delivers it to the upstream reservoir.

To ensure uniform and stable flow within the test section, a honeycomb flow straightener was installed at the outlet of the inlet reservoir. Additionally, the connection between the inlet reservoir and the test section was contracted at a 2:1 ratio to minimize flow disturbances. The inlet reservoir also serves as a settling chamber, allowing water to pass through a flow regulation section before entering the test section, thereby improving flow uniformity for PIV measurements.

The system is equipped with a filtration unit to remove foreign particles and debris from the water in the reservoirs. To minimize thermal interactions between the water channel and the particle circulation system, the laboratory temperature was maintained at  $22^\circ\text{C}$ . Furthermore, to prevent interference from sunlight on the laser beam, the laboratory windows were covered with special blackout curtains. A schematic view of the test channel is presented in Figure 1 (Gölbaşı, 2015).



Figure 1. Test channel

The **Particle Image Velocimetry (PIV)** technique generally involves two main stages: **flow visualization** and **image processing**. To track the flow, small tracer particles are introduced into the experimental domain. These particles are illuminated twice in rapid succession by a light source positioned over the measurement plane. The time interval between consecutive illuminations is adjusted according to the **mean flow**

**velocity** and the **magnification scale**. During this interval, the particles move according to the local flow velocity, and the light they scatter is captured on two separate frames by a **high-resolution camera** positioned perpendicular to the light sheet. The recorded PIV images are subsequently digitized and transferred to a computer for further analysis. **Figure 2** illustrates the working principle of the PIV technique.

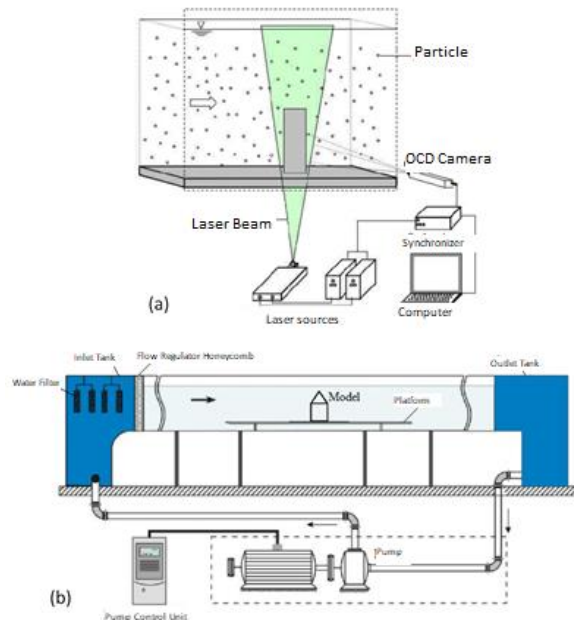


Figure 2. (a) PIV working principle (b) schematic view of the water channel (Gölbaşı, 2015)

In the experiments, **three different building models** fabricated from transparent acrylic were employed to investigate flow characteristics. The water level in the test section was maintained at a constant **0.45 m**, and the **front edge of the platform** was beveled to prevent flow disturbances. The models were positioned **1.5 m downstream of the channel inlet** to minimize turbulence effects. Experiments were conducted under conditions where the **free-stream flow velocity** was set to **210 mm/s**.

#### Top View Surface Measurements

As illustrated in Figure 3(a), the camera is positioned opposite the channel, while a laser is placed in front of the building to capture its top view. A mirror inclined at  $45^\circ$  is installed in front of the camera to complete the experimental setup. The positions of both the camera and the mirror are shown in Figure 3(b). The symmetry plane considered for the top view is taken at  $y/H = 0$ , as depicted in Figure 3(c) (Gölbaşı, 2015).

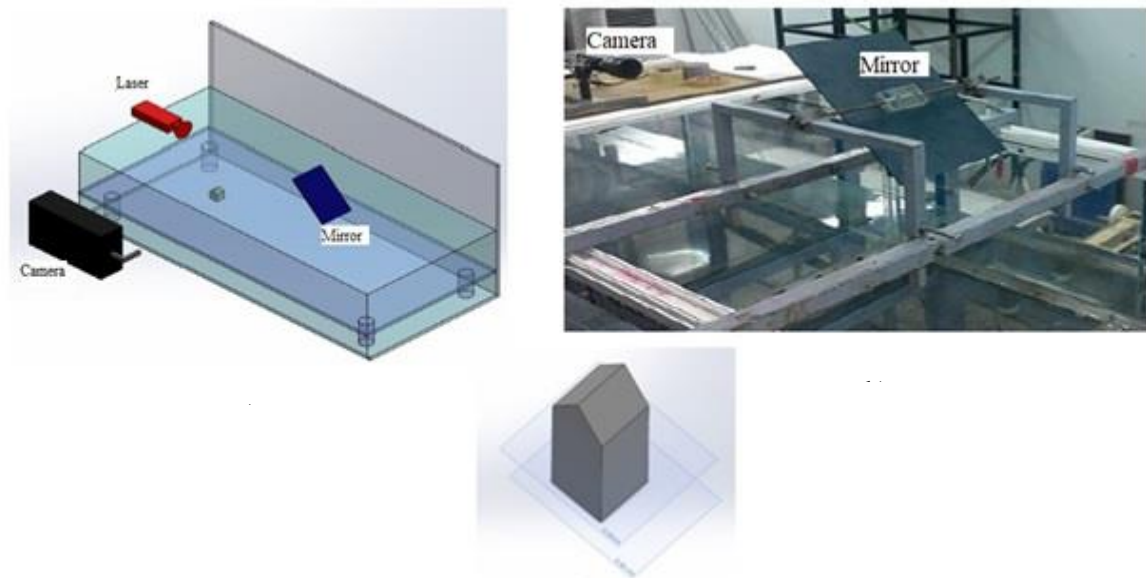


Figure 3. (a) Arranged view of the apparatus for top view (b) Camera and mirror positions for top view (c) Top view measurement surface simulation

### Results and Discussion

This study calculated the average velocities of five hundred photographs. Streamlines consist of a series of lines that are the tangents of the local velocity vectors at any given moment. Vorticity is also a measure of the rotation of flow particles. Vorticity values for each measurement surface were determined using the average velocities.

The flow structure formed around the buildings, streamlines  $\langle \psi \rangle$ , velocity distribution, and dimensionless vorticity contour lines  $\langle \omega \rangle$  were obtained from

experimental results. While velocity vectors show the flow distribution and direction in experimental data, streamlines facilitate the understanding of instantaneous flow data. The turbulent boundary layer formed the average equivalent velocity curves. Figures 4(a), (b), (c), and (d) show the schematic experimental placements of buildings placed at a distance from each other and the shape placements of the building model, respectively.

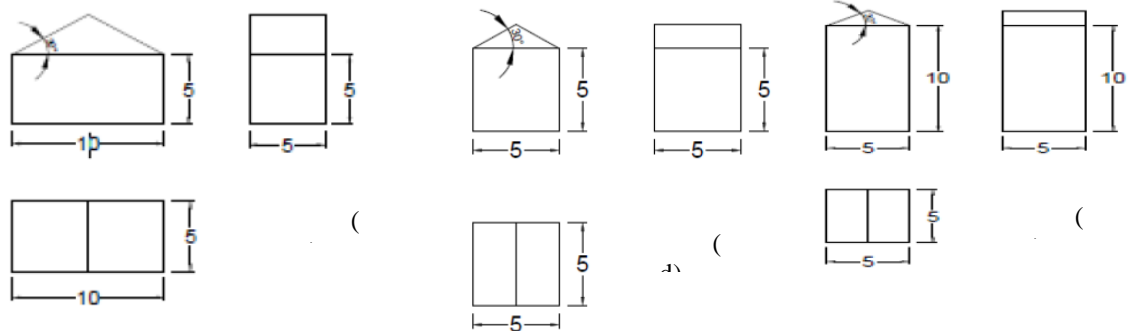
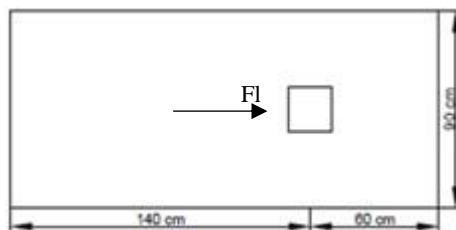
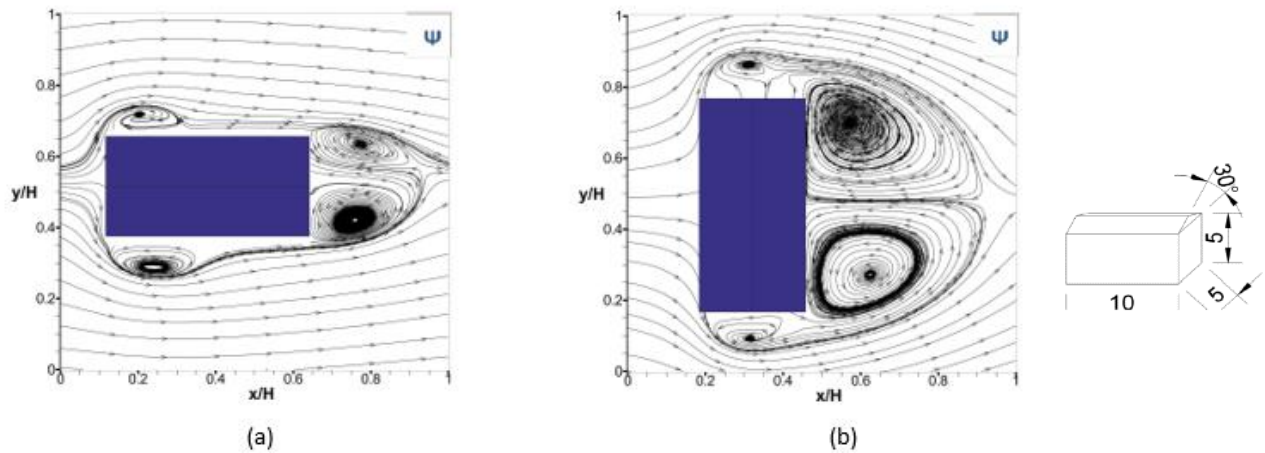


Figure 4. Display of roofed models (a) schematic (b) experimental (c) roofed wide building model (d) roofed short building model (e) roofed long building model

### Experimental Results



**Figure 5.** Time-averaged streamlines  $\langle \psi \rangle$  on the symmetry plane  $y/H = 0.5$  for the flow around the building model with dimensions  $10 \text{ cm} \times 5 \text{ cm} \times 5 \text{ cm}$ .

Figures 5 (a) and (b) illustrate the streamlines of the flow around a rectangular structure. In Figure 5 (a), the structure is positioned parallel to the flow direction, where the streamlines form a stagnation region at the front of the structure and a distinct separation and recirculation zone behind it. The recirculation region formed at the rear of the structure causes the flow to change direction around the body, leading to the formation of two vortex structures. This indicates that the flow accelerates significantly near the corners of the structure and that the pressure distribution becomes unbalanced.

In Figure 5 (b), the structure is rotated  $90^\circ$ , thus becoming perpendicular to the flow direction. In this case, the flow characteristics change significantly, and two large vortex regions form behind the structure. These vortex structures, located in the upper and lower regions, indicate that the flow separates into two main circulation zones after impinging on the surface of the body. Additionally, pressure accumulation increases at the front of the structure, while a wide low-pressure region develops at the rear. This suggests that the flow separation occurs earlier and that the drag force increases in this configuration.

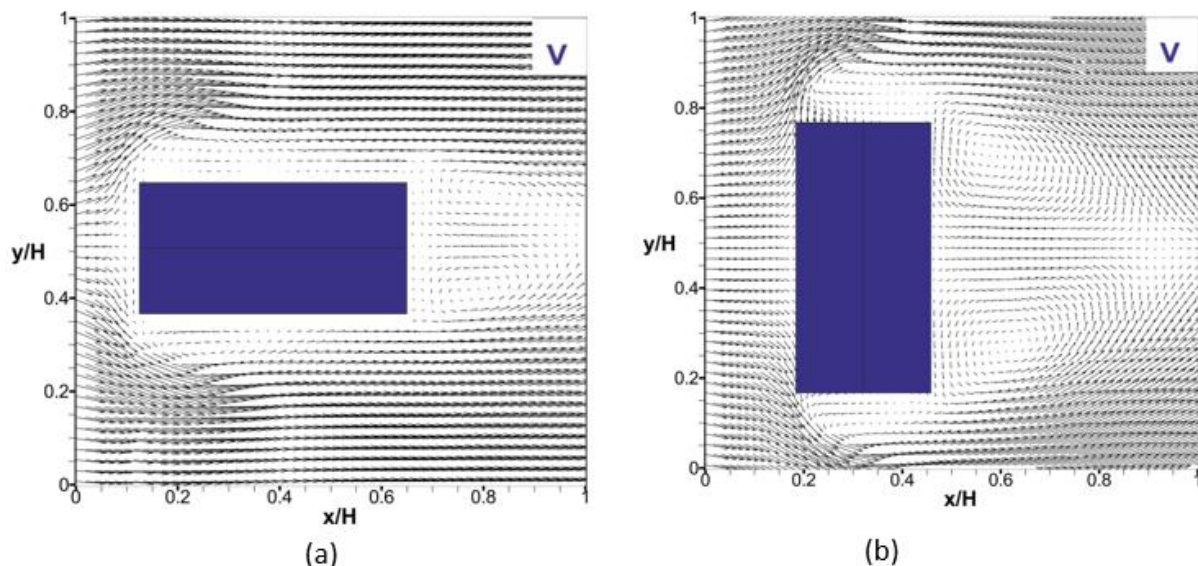


**Figure 6.** Time-averaged velocity distribution  $\langle V \rangle$  on the symmetry plane  $y/H = 0.5$  for the flow around the building model with dimensions  $10 \text{ cm} \times 5 \text{ cm} \times 5 \text{ cm}$ .

Figures 6(a) and (b) illustrate the effects of the orientation of a wide, rectangular-plan building with a roof on the flow characteristics under wind conditions. In Figure 6(a), the long side of the building is positioned parallel to the flow direction, and in this configuration, the streamlines are observed to advance more steadily along the building surface. In this case, the flow forms a limited stagnation region on the front face of the

building and is directed toward the side surfaces without causing large-scale separations. As the flow moves smoothly around the structure, the wake region behind the building develops in a narrow form, and low-velocity gradients are concentrated in localized areas. This indicates that the aerodynamic drag forces acting on the structure are relatively low.

When the building is rotated by  $90^\circ$ , as shown in Figure 6(b), a distinct stagnation region develops on the



broad surface perpendicular to the flow direction, accompanied by abrupt decreases in velocity vectors. Due to the high resistance presented by this surface, the flow undergoes strong deflections in the upward, downward, and lateral directions. As a result of these deviations, the turbulence intensity increases, and flow separation occurs earlier. As the separations grow, a large wake region develops behind the structure, the low-pressure zones deepen, and consequently, the drag component increases significantly. Moreover, distinct vortex structures emerge near the corner regions, which enhance

both temporal and spatial fluctuations within the flow field.

A comparison of both configurations reveals that in Figure 6(a), where the building is oriented parallel to the flow direction, the flow continuity remains more stable, the wake region is narrower, and the turbulence characteristics of the flow are weaker. In contrast, in Figure 6(b), due to the impingement of the flow on a wide frontal surface, pronounced pressure gradients, higher turbulence levels, and a more extensive wake region are observed.

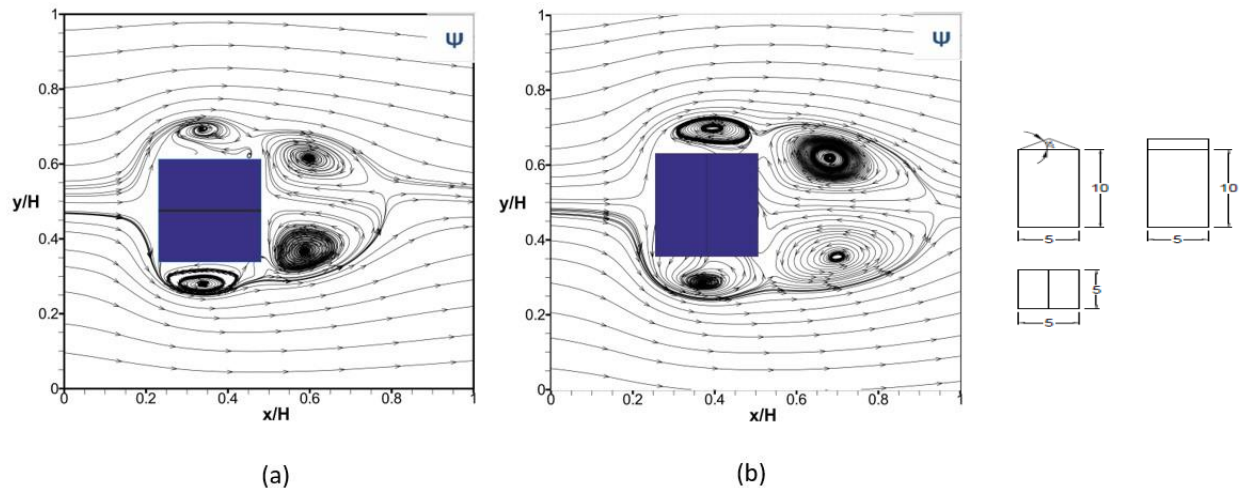


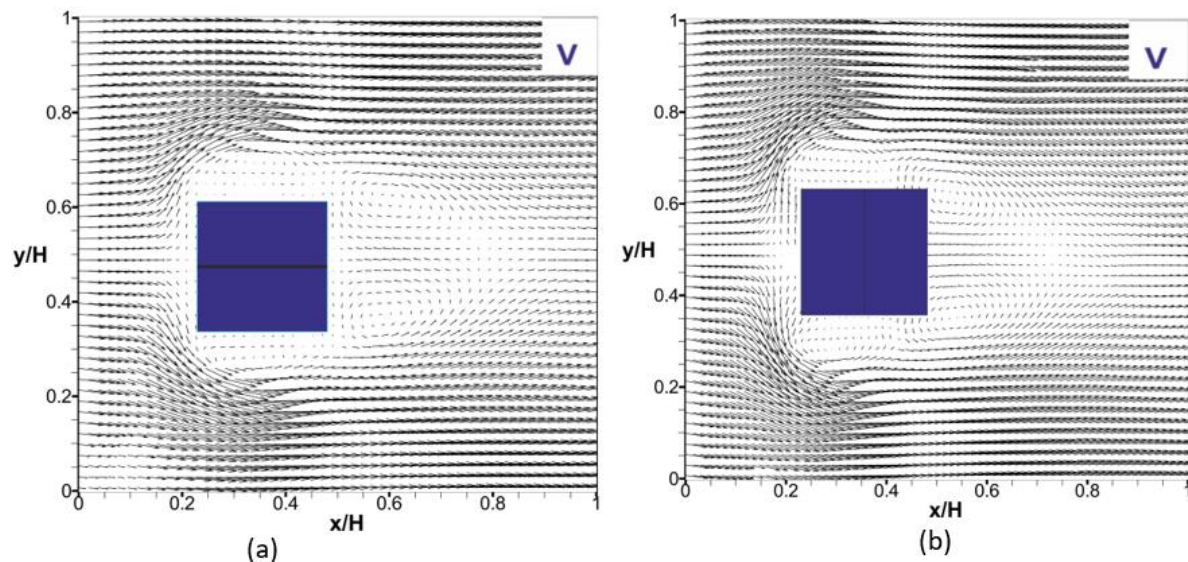
Figure 7. Time-averaged streamlines  $\langle \psi \rangle$  on the symmetry plane  $y/H = 0.5$  for the flow around the building model with dimensions  $5 \text{ cm} \times 5 \text{ cm} \times 10 \text{ cm}$ .

Figures 7(a) and (b) illustrate the effects of different orientations of a long building with a square cross-section on the flow structure relative to the flow direction. In Figure 7(a), the short side of the building is positioned parallel to the flow direction. In this case, the streamlines, after contacting the building surface, induce flow separation on both the upper and lower surfaces, resulting in the formation of asymmetric vortex regions behind the structure. The more intense vortical structures observed in the lower part of the building indicate an increase in near-ground turbulence energy. As the flow passes along the side faces of the building, slight deviations are observed, and the wake region appears relatively confined to a narrower area. This indicates that the short building dimension limits the length of the wake region by bringing the flow reattachment point closer to the rear of the building.

In Figure 7(b), the building is rotated by  $90^\circ$ , presenting a wider surface facing the incoming flow. In this configuration, a distinct stagnation region forms at the point where the streamlines meet the building sur-

face, and the flow exhibits sharper deviations both upward and downward. The recirculation zone expands, and multiple vortical structures are observed to overlap within the wake region. The formation of larger-scale vortices, particularly in the upper part of the building, contributes to increased aerodynamic loads and enhances the potential for turbulence-induced structural vibrations. The elongation of the wake region and the increase in vortex density are associated with the abrupt momentum loss of the flow impacting the wide surface, indicating an increase in the drag component.

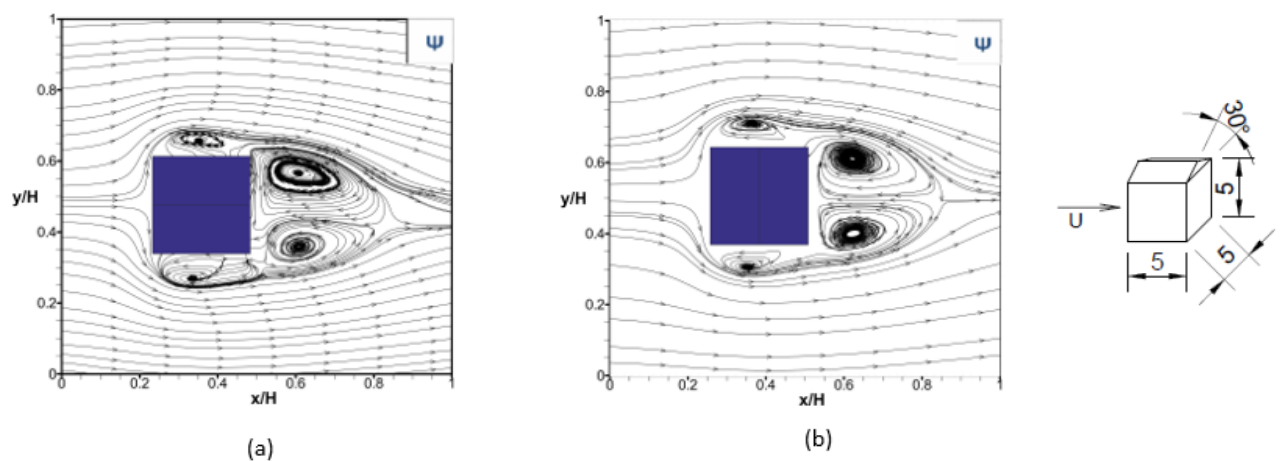
A comparison of both configurations shows that, in the parallel orientation of the short building, the wake region remains more compact and the vortical structures develop on a smaller scale. In contrast, in the  $90^\circ$  rotated configuration, both the wake length and vortex intensity increase, leading to more complex turbulent structures in the flow field. These results demonstrate that building dimensions and orientation have a critical influence on flow topology, wake characteristics, and the distribution of aerodynamic loads.



**Figure 8.** Time-averaged velocity distribution  $\langle V \rangle$  on the symmetry plane  $y/H = 0.5$  for the flow around the building model with dimensions  $5 \text{ cm} \times 5 \text{ cm} \times 5 \text{ cm}$ .

Figure 8(a) shows the velocity vector distribution of a square-section tall building model placed in the flow field in its reference position (original orientation). When the flow impacts the front face of the building, a distinct stagnation zone forms, and the flow lines separate around the top and bottom edges as the flow continues. Behind the building, a wake region with low velocities is observed. This region is characterized by vortex structures generated as the flow separates from the building's corners.

Figure 8(b) gives the same building model rotated by  $90^\circ$ . In this case, the interaction between the flow and the building changes, and the location and extent of the stagnation zone on the front face differ. The change in building orientation affects the deflection angle of the flow and the symmetry of the wake region behind the building. In the rotated model, the flow lines merge more smoothly, and the turbulence effects in the rear region are somewhat reduced.



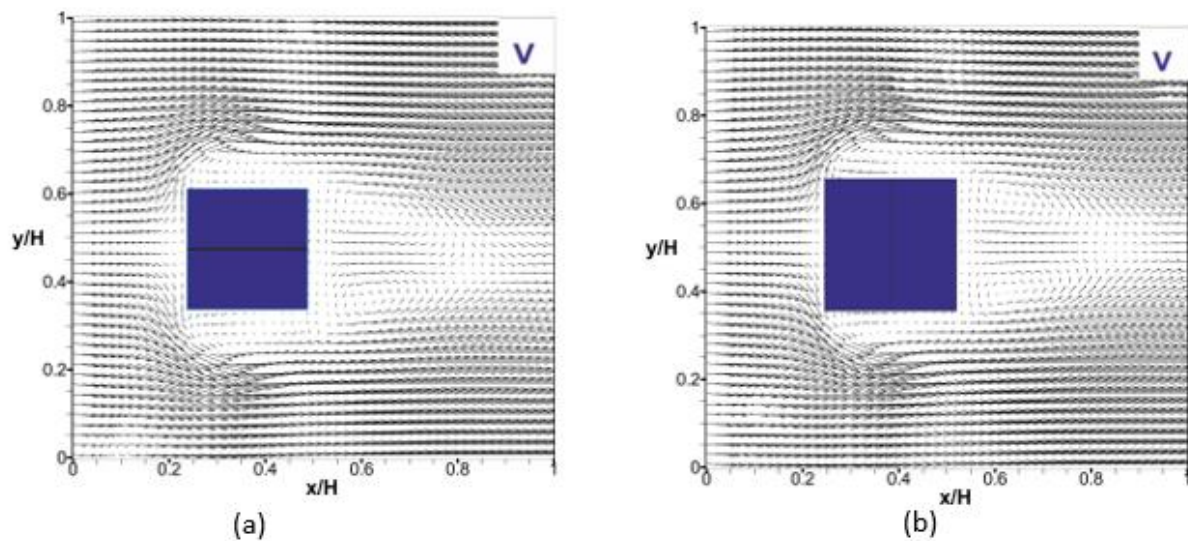
**Figure 9.** Time-averaged streamlines  $\langle \psi \rangle$  on the symmetry plane at  $y/H = 0.5$  for the flow around the  $5 \text{ cm} \times 5 \text{ cm}$  building model.

Figure 9(a) indicates the streamlines around the square-section short building model. When the flow impacts the front face of the building, flow separation occurs, and a distinct recirculation zone forms behind the building. Within this region, two counter-rotating vortex structures are observed. These vortices, occurring along the top and bottom edges, develop in low-velocity areas after the flow separates from the building. The streamlines in the wake region exhibit a complex

pattern under the influence of these vortices, showing irregular flow characteristics up to the reattachment point.

Figure 9(b) presents the same building model rotated by  $90^\circ$ . In this case, significant changes occur in the distribution of streamlines and the positions of the vortical structures. In the rotated model, the separation regions along the top and bottom edges become more symmetric, and the length of the recirculation zone behind the building is reduced. This indicates that the

flow separates more smoothly from the building, and the turbulence effects in the wake region are relatively diminished.



**Figure 10.** Time-averaged velocity distribution  $\langle V \rangle$  for the flow around a building model with dimensions  $5\text{ cm} \times 5\text{ cm} \times 5\text{ cm}$ , with a symmetry surface  $y/H = 0.5$ .

Figure 10(a) illustrates the velocity vector field obtained for the reference orientation of the short building model with a square cross-section. When the flow strikes the front surface of the building, a distinct stagnation zone forms, and from this zone onwards, the flow lines are directed around the building, passing through the upper and lower edges. A wake region with low velocities is observed behind the building. In this region, the flow velocity decreases, and recirculating flow with vortex structures is noticeable.

Figure 10(b) exhibits the same building model rotated by  $90^\circ$ . Changing the orientation of the building significantly affects the interaction of the flow with the building surfaces and the locations of the separation regions. In the rotated state, the distribution of the stagnant zone on the front surface has changed, and it can be seen that the flow separation behind the building occurs in a narrower area. This indicates that the flow separates from the building in a more balanced manner and that the recirculation effects in the rear area are reduced.

#### General Results And Evaluation

**1-** As the wind impacts and separates around the edges and corners of buildings, recirculation zones develop at the front façades, along the side walls, at the rear, and over the roof regions. Turbulence intensities increase significantly in the shear layers that separate these recirculation zones from the free-stream flow.

**2-** As one moves from the symmetry axis toward the side edges, the boundary layer thickness decreases, while the jet flow in the downstream region becomes lower in energy. This phenomenon causes the separation region behind the building models to shorten progressively toward the side edges.

**3-** Regions of high turbulent kinetic energy are formed in the wake vortices behind the buildings, which correspond to the recirculation zones. Moving

downstream from the rear of the buildings, turbulent kinetic energy levels increase near these vortex regions and gradually decrease with distance from them.

**4-** When the  $10\text{ cm} \times 5\text{ cm} \times 5\text{ cm}$  building model is rotated, the vortices formed behind the building increase noticeably in size. Both the width and thickness of these vortices are observed to grow. Furthermore, a significant portion of the flow around the building is affected by these recirculation zones.

**5-** When the  $5\text{ cm} \times 5\text{ cm} \times 10\text{ cm}$  building model is rotated, similar to the  $10\text{ cm} \times 5\text{ cm} \times 5\text{ cm}$  model, the vortices formed behind the building become significantly larger, with increases observed in both their width and thickness.

**6-** When the  $5\text{ cm} \times 5\text{ cm} \times 5\text{ cm}$  building model is rotated, no significant changes are observed in the flow characteristics.

#### References:

1. Albuquerque, D. P., Sandberg, M., Linden, P. F., & da Graça, G. C. (2020). Experimental and numerical investigation of pumping ventilation on the leeward side of a cubic building. *Building and Environment*, 179, 106897.
2. Bagheri, M., Ghanbari Barfeh, D., Karami, M., Delfani, S., & Hafezi, M. (2023). Experimental investigation of buoyancy-driven natural ventilation in a building with an atrium using particle image velocimetry (PIV) method. *Advances in Building Energy Research*, 17(5), 536-553.
3. Blocken, B. (2014). 50 years of Computational Wind Engineering: Past, present and future. *Journal of Wind Engineering and Industrial Aerodynamics*, 129, 69-102.
4. Gölbasi, D. (2015). *Experimental and theoretical investigation of heat transfer and flow structures over buildings with different geometries in urban areas* (Doctoral dissertation, Cumhuriyet University, Sivas, Turkey).



5. Han, D., Zhang, T., Qin, Y., & Tan, Y. (2022). Experimental study on thermal plume characteristics of building façades based on PIV technology. *Sustainable Cities and Society*, 77, 103589.
6. Kim, B., Tse, K. T., Yoshida, A., Chen, Z., Van Phuc, P., & Park, H. S. (2019). Investigation of flow visualization around linked tall buildings with circular sections. *Building and Environment*, 153, 60-76.
7. Liu, J., Hui, Y., Yang, Q., & Tamura, Y. (2021). Flow field investigation for aerodynamic effects of surface mounted ribs on square-sectioned high-rise buildings. *Journal of Wind Engineering and Industrial Aerodynamics*, 211, 104551.
8. Liu, J., Hui, Y., Yang, Q., & Zhang, R. (2023). LES evaluation of the aerodynamic characteristics of high-rise building with horizontal ribs under atmospheric boundary layer flow. *Journal of Building Engineering*, 71, 106487.
9. Liu, J., Liu, J., & Li, J. (2024). PIV experimental study on natural convective flows at high Rayleigh numbers in industrial buildings. *Building and Environment*, 256, 111460.
10. Reyes, V. A., Sierra-Espinosa, F. Z., Moya, S. L., & Carrillo, F. (2015). Flow field obtained by PIV technique for a scaled building-wind tower model in a wind tunnel. *Energy and Buildings*, 107, 424-433.
11. Setio, H. D., Sarli, P. W., Sanjaya, Y., & Priambodo, D. (2020). Experimental Study of Wind Flow in a Street Canyon between High-Rise Buildings Using PIV. *Journal of Engineering and Technological Sciences*, 52(5), 639-650.
12. Sugahara, A., Kotani, H., Momoi, Y., Yamana, T., Sagara, K., & Fujiwara, R. (2017). PIV measurement and CFD analysis of airflow around building roof with various building installations. *International Journal of Ventilation*, 16(3), 163-173.
13. Tominaga, Y., Akabayashi, S. I., Kitahara, T., & Arinami, Y. (2015). Air flow around isolated gable-roof buildings with different roof pitches: Wind tunnel experiments and CFD simulations. *Building and Environment*, 84, 204-213.